Optimization of Dynamic Response using Temporal Spectral Element Method

Mohammad Kurdi* and Philip Beran †
Air Force Research Laboratory, WPAFB OH 45433.

The design of systems for dynamic response may involve constraints that need to be satisfied over an entire time interval or objective functions evaluated over the interval. Efficiently performing the constrained optimization is challenging, since the typical response is implicitly linked to the design variables through a numerical integration of the governing differential equations. Evaluating constraints is costly, as is the determination of sensitivities to variations in the design variables.

In this paper, we investigate the application of a temporal spectral element method to the optimization of transient and time-periodic responses of fundamental engineering systems. Through the spectral discretization, the response is computed globally, thereby enabling a more explicit connection between the response and design variables and facilitating the efficient computation of response sensitivities. Furthermore, the response is captured in a higher order manner to increase analysis accuracy.

Two applications of the coupling of dynamic response optimization with the temporal spectral element method are demonstrated. The first application, a one-degree-of-freedom, linear, impact absorber, is selected from the auto industry, and tests the ability of the method to treat transient constraints over a large-time interval. The second application, a related mass-spring-damper system, shows how the method can be used to obtain work and amplitude optimal time-periodic control force subject to constraints over a periodic time interval.

I. Introduction

Many engineering structures are subject to transient loading conditions. These structures must handle load variations for an entire time interval. To enforce the time-dependent constraints, the response needs to be evaluated accurately for an entire interval without missing any of the response extrema. Additionally, this evaluation needs to be efficient when an optimum design of the structure is sought because the objective, constraints and their sensitivities will need to be recomputed for each configuration visited by the optimizer.

The overwhelming majority of numerical techniques used to compute time-dependent responses are based on finite-difference schemes. In these methods, the solution of the governing second order differential equation is time-marched from the initial condition using small time steps until the dynamics reach a converged state. Here the time step size is crucial to the stability and accuracy of the computation and may limit its efficiency. Additionally, in a gradient-based optimization search, the sensitivity of the response to design variables is required. The sensitivity can be computed using direct differentiation or adjoint method by defining a Lagrange multiplier [1, 2]. This computation is convoluted because the response is not explicit in the design variables. In both methods, the response sensitivity computation is hindered by another integration of the governing differential equations.

In the review by Kang et al. [3], the authors noted the advantage of using a finite element discretization of the time parameter. The attractive feature of the time finite element method [4, 5] is that it transforms the governing differential equation into an algebraic equation. This has the advantage of obtaining a more explicit connection of the response to the design variables, which in turn enables more efficient computation

*NRC Research Associate, AFRL/RBSD, 2210 8th Street, Bldg 146, WPAFB, OH 45433. mhkurdi@gmail.com. AIAA Member.
†Principal Research Aerospace Engineer, AFRL/RBSD. AIAA Associate Fellow.

of the response sensitivity. In this paper, we use temporal spectral element method to discretize the time-dependent differential equation. The spectral element method, first introduced by Patera [6], combines the local flexibility of the finite element method with the accuracy of spectral methods. Within each element, a high order Lagrange polynomial is interpolated at time grid points corresponding to zeros of Gauss-Lobatto-Legendre (GLL) polynomials. The solution of the differential equation is computed for a monolithic time interval which includes transient and steady-state response [7].

Early studies on the optimization of structures subject to transient loads goes back to the 1970s [8, 9]. This branch of optimization is referred to in the literature as dynamic response optimization [3]. Here, the time-dependent responses need to be evaluated for each iteration of the design variables and the constraints enforced for an entire time interval. There are several methods to apply time-dependent constraints. In an early work, Venkayya [10] applied the constraint only at the global minimum of the response. Another approach enforces the constraints at closely spaced points such that violation at intermediate points is unlikely [11]. This approach increases the number of constraints substantially. The optimization cost also increases because of the need to compute sensitivities of these constraints during the optimizer iterations. A more efficient procedure is to enforce the constraints only at all the local extrema of the response critical to the design. This reduces the number of constraints and the resulting reduction in number of sensitivities calculations of the constraints with respect to the design variables [2, 12, 13].

In this paper we use the temporal spectral element method for computing the time-dependent constraints responses to enable efficient dynamic response optimization. The discretization transforms the time dependence of the response into an explicit algebraic form. Since the solution is already available at the GLL grid points, we compare the optimization cost of enforcing the constraints at these points with enforcing them only at the local extrema of the responses, where the extrema are identified using a one dimensional optimization search method. Two applications are described. The first application, derived from the auto industry, demonstrates the method efficiency and accuracy for the transient response of linear systems. The second application, is motivated by path control force design of micro air vehicles, demonstrate the method for systems with periodic steady-state response.

II. Formulation of Dynamic Response Optimization Problem

The dynamic response optimization problem is to find the design variable vector $\boldsymbol{b}$ which

$$\begin{aligned} &\text{minimize} \quad c(\boldsymbol{b}, \boldsymbol{z}(t), \dot{\boldsymbol{z}}(t), \ddot{\boldsymbol{z}}(t), t), \\ &\text{subject to} \\ &\qquad g_i(\boldsymbol{b}, \boldsymbol{z}(t), \dot{\boldsymbol{z}}(t), \ddot{\boldsymbol{z}}(t), t) \leq 0, \quad i = 1, ..., n \quad \forall t \in [0, T], \end{aligned} \tag{1}$$

where g_i is constraint number i and t is the time parameter and $\boldsymbol{z}$ is displacement vector which is the solution to

$$\begin{aligned} &\mathbf{M}\ddot{\boldsymbol{z}} + \mathbf{C}\dot{\boldsymbol{z}} + \mathbf{K}\boldsymbol{z} = \boldsymbol{f}, \\ &\boldsymbol{z}(0) = \boldsymbol{z}_0 \qquad \dot{\boldsymbol{z}}(0) = \dot{\boldsymbol{z}}_0, \end{aligned} \tag{2}$$

where $\mathbf{M}$, $\mathbf{C}$, $\mathbf{K}$ are the mass, damping and stiffness matrices. Note that the function g is an aggregate of the time-dependent response and the set-point of design constraint, consequently we refer to g as being time-dependent due to the time dependency of the response and not the design constraint point. Typically the solution of (2) is computed using time stepping schemes. In our approach we compute the response using a monolithic time approach. This transforms the time-dependent differential equation to an algebraic form and eliminates direct dependence on time. In the following we describe the temporal spectral element method which is used to apply the transformation.

III. Temporal Spectral Element Method

The spectral element (SE) method is applied to a set of linear first-order differential equations. Higher order unsteady terms such as in (2) can easily be tackled by transforming to first-order form. The coupled set of differential equations is,

$$\frac{\mathrm{d}x}{\mathrm{d}t} + \mathbf{A_s}x = f(x,t), \tag{3}$$

where x represents the collocated dependent variables $x \in R^{N_v}$, N_v is the number of dependent variables, time t is the independent variable, and $f(x,t)$ is a nonlinear function of x which can be time-dependent. The equations are coupled through the matrix $\mathbf{A_s}$, which is assumed to be time invariant.

Ordinarily, initial conditions need to be specified in simulating (3). However, this is generally not the case when cyclic solutions of (3) are sought, i.e., those that are time-periodic in response to a time-periodic forcing function, $f(\omega t, x)$, with a circular frequency, ω.

III.A. Transient Analysis

Each dependent variable can be discretized in time using spectral elements [14], where the approximate m^{th} order solution in each element is:

$$\hat{x}^{(j)}(\zeta) = \sum_{k=0}^{m} x^{(j)}(\zeta_k)\psi_k^{(j)}(\zeta). \tag{4}$$

Here $\psi_k^{(j)}$ represents the Lagrange polynomial of order k in element j, ζ_k are the zeros of the Lobatto-Legendre polynomials defined on the interval $\zeta \in [-1,1]$ and $x^{(j)}(\zeta_k)$ are the unknown nodal values placed at ζ_k for element j. See Fig. (1), where the physical time domain $t \in [t_j, t_{j+1}]$ is transformed to the ζ domain for each element. The Lobatto polynomials L_{o_i} are a set of orthogonal polynomials that can be defined as the derivatives of the Legendre polynomials [15], L_i:

$$L_{o_i}(\zeta) \equiv L_{i+1}^{'}(\zeta), \tag{5}$$

where the Legendre polynomials are defined explicitly as

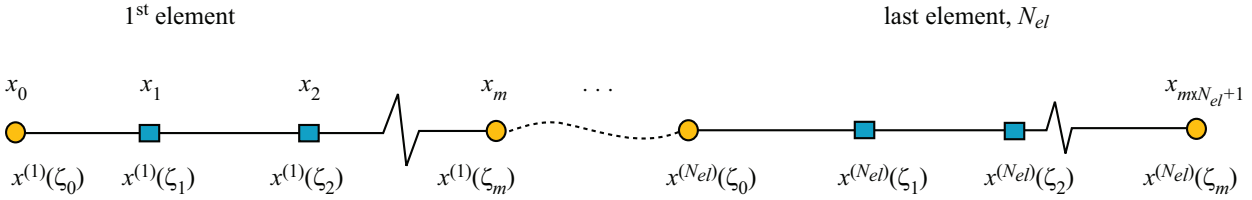

Figure 1. Discretization of the time domain into N_{el} elements represented by an m order Lagrange polynomial within each element. Nodes of each element are placed at zeros of Lobatto polynomials.

$$L_i(\zeta) = \frac{1}{2^i i!}\frac{\mathrm{d}^i(\zeta^2-1)^i}{\mathrm{d}\zeta^i}. \tag{6}$$

We review the development of SE here for completeness. Substituting the trial solution $\hat{x}^{(j)}$ into the differential equation (3) and minimizing the residual in each element using the Bubnov-Galerkin method [16] we have (assume A_s is scalar for now):

$$\sum_{j=1}^{N_{el}} \int_{-1}^{1} v(\zeta)\Big[\frac{\mathrm{d}\hat{x}^{(j)}}{\mathrm{d}\zeta} + \frac{h^{(j)}}{2}\Big\{A_s\hat{x}^{(j)} - f^{(j)}(\hat{x}^{(j)},\zeta)\Big\}\Big]\,\mathrm{d}\zeta = 0, \tag{7}$$

where $h^{(j)}$ is the width of element j and $v(\zeta)$ is a weighting function taken as the p^{th} Lagrange polynomial, $\psi_p^{(j)}$. Integrating by parts we find for $p = 0, \ldots, m$:

$$\sum_{j=1}^{N_{el}} \Big[\hat{x}^{(j)}\psi_p^{(j)}\Big|_{-1}^{1} - \int_{-1}^{1}\big(\hat{x}^{(j)}\frac{\mathrm{d}\psi_p^{(j)}}{\mathrm{d}\zeta} - \frac{h^{(j)}}{2}\Big\{A_s\hat{x}^{(j)}\psi_p^{(j)} - f^{(j)}(\hat{x}^{(j)},\zeta)\psi_p^{(j)}\Big\}\big)\mathrm{d}\zeta\Big] = 0. \tag{8}$$

Exploiting the property of Lagrange polynomials, (8) is efficiently integrated using Gaussian quadrature rule according to:

$$\int_{-1}^{1} I \mathrm{d}\zeta = \sum_{q=0}^{m} I(\zeta_q)\omega_q, \tag{9}$$

where I is a generic function of ζ and ω_q is the Gaussian quadrature weight at node q. This gives the following compact matrix formulation for each element:

$$\mathbf{\Psi} \begin{Bmatrix} x(\zeta_0) \\ \vdots \\ x(\zeta_m) \end{Bmatrix}^{(j)} = A_s \mathbf{I}_\omega^{(j)} \begin{Bmatrix} x(\zeta_0) \\ \vdots \\ x(\zeta_m) \end{Bmatrix}^{(j)} - \mathbf{I}_\omega^{(j)} f^{(j)}, \tag{10}$$

where

$$\mathbf{\Psi} = \begin{bmatrix} \frac{\mathrm{d}\psi_0}{\mathrm{d}\zeta}\big|_{\zeta_0}\omega_0 + 1 & \frac{\mathrm{d}\psi_0}{\mathrm{d}\zeta}\big|_{\zeta_1}\omega_1 & \dots & \frac{\mathrm{d}\psi_0}{\mathrm{d}\zeta}\big|_{\zeta_m}\omega_m \\ \frac{\mathrm{d}\psi_1}{\mathrm{d}\zeta}\big|_{\zeta_0}\omega_0 & \frac{\mathrm{d}\psi_1}{\mathrm{d}\zeta}\big|_{\zeta_1}\omega_1 & \dots & \vdots \\ \vdots & \dots & \dots & \frac{\mathrm{d}\psi_{m-1}}{\mathrm{d}\zeta}\big|_{\zeta_m}\omega_m \\ \frac{\mathrm{d}\psi_m}{\mathrm{d}\zeta}\big|_{\zeta_0}\omega_0 & \dots & \frac{\mathrm{d}\psi_m}{\mathrm{d}\zeta}\big|_{\zeta_{m-1}}\omega_{m-1} & \frac{\mathrm{d}\psi_m}{\mathrm{d}\zeta}\big|_{\zeta_m}\omega_m - 1 \end{bmatrix}, \tag{11}$$

and

$$\mathbf{I}_\omega = \frac{h^{(j)}}{2} \begin{bmatrix} \omega_0 & 0 & \dots & 0 \\ 0 & \omega_1 & \dots & 0 \\ \vdots & \vdots & \ddots & \vdots \\ 0 & 0 & \dots & \omega_m \end{bmatrix}. \tag{12}$$

In (11), the first and last diagonal elements of differentiation matrix $\mathbf{\Psi}$ have an additional term (=1) due to the first term in (8). After enforcing the essential inter-element continuity

$$x^{(j)}(\zeta_m) = x^{(j+1)}(\zeta_0), \tag{13}$$

the assembly of a global matrix from (10) for N_{el} spectral elements yields a compact, Galerkin projection governing the approximate solution in time (one dependent variable):

$$\mathbf{L}_c X_c = A_s \mathbf{L}_\omega X_c - \mathbf{L}_\omega F(X_c), \tag{14}$$

where $\mathbf{L}_c$ and $\mathbf{L}_\omega$ are the global differentiation and weight matrices, F is the global weighted form of the excitation and

$$X_c = \begin{bmatrix} x\big|_{t_0} & x\big|_{t_1} & \dots & x\big|_{t_{m\times N_{el}+1}} \end{bmatrix}^T, \tag{15}$$

is the SE solution of the dependent variable x collocated at all nodal times (redundant shared elements nodes are removed using (13)). It should be noted that the initial condition is applied by replacing the first row and column of $\mathbf{L}_c$ with zeros except for the first element, which is replaced with one. Also, the first element in $\mathbf{L}_\omega$ is replaced with zero and the first element in $-\mathbf{L}_\omega F$ is replaced with the value of x at $t = 0$. The SE solution X_c in (14) can then be computed using iterative methods. However, for a strictly time-dependent forcing function (not function of X_c) both direct and iterative methods can be used, see Section III.C.

III.B. Periodic Cyclic Analysis

In some problems, the interest lies in the steady-state time solution, where the response is time-periodic with a period, $T = 2\pi/\omega$, equal to the period of the forcing function. This occurs in damped systems with periodic forcing functions and in self-excited nonlinear systems exhibiting limit cycle oscillations (LCOs).

In these problems we are interested in the steady-state periodic solution only, where the time cycle is discretized spectrally in the same way as in the transient solution, however, assembly of global matrices $\mathbf{L}_c$ and $\mathbf{L}_\omega$ is different. Here the initial conditions do not affect the long term periodic solution. Additionally,

periodicity of the array of elements is enforced by requiring that the end node in the last element to be the initial node of the first element:

$$x^{(1)}(\zeta_0) = x^{(N_{el})}(\zeta_m). \tag{16}$$

Contributions to the end node in the last element are added to contributions from first element. Consequently the last row and column of $\mathbf{L}_c$ are added to their counterpart in the first row and column. Therefore, the solution vector, X_c, becomes

$$X_c = \left[x\big|_{t_0} \quad x\big|_{t_1} \quad \dots \quad x\big|_{t_{m\times N_{el}}} \right]^T. \tag{17}$$

III.C. Global Assembly and Solution

A number of dependent variables, N_v, can be handled through spatial connectivity matrix $\mathbf{A}_s$ of size $N_v \times N_v$. Here, the tensor product gives the global form of (14):

$$(\mathbf{I} \otimes \mathbf{L}_c)X_{cg} = (\mathbf{A}_s \otimes \mathbf{L}_\omega)X_{cg} - (\mathbf{I} \otimes \mathbf{L}_\omega)F_{cg}(X_{cg}), \tag{18}$$

where $\mathbf{I}$ is the identity matrix of size $N_v \times N_v$ and X_{cg} is a collocation of all dependent variables at nodal times grouped by their corresponding independent variables, N_v. For transient solution X_{cg} takes the form:

$$X_{cg} = \left[\begin{Bmatrix} x_1\big|_{t_0} \\ x_1\big|_{t_1} \\ \vdots \\ x_1\big|_{t_{m\times N_{el}+1}} \end{Bmatrix}^T \quad \dots \quad \begin{Bmatrix} x_{N_v}\big|_{t_0} \\ x_{N_v}\big|_{t_1} \\ \vdots \\ x_{N_v}\big|_{t_{m\times N_{el}+1}} \end{Bmatrix}^T \right]^T. \tag{19}$$

A compact form of (18) becomes

$$\mathbf{J}X_{cg} = -\mathbf{L}_{\omega g}F_{cg}(X_{cg}), \tag{20}$$

where

$$\mathbf{J} = \mathbf{L}_{cg} - \mathbf{A}_{cg}. \tag{21}$$

The solution X_{cg} of (20) can be computed using Newton's method. By identifying a residual R we can write (20) as

$$R = \mathbf{J}X_{cg} + \mathbf{L}_{\omega g}F_{cg}(X_{cg}). \tag{22}$$

A first order Taylor series expansion of the nonlinear formula (22) gives

$$R^{\nu+1} = R^{\nu} + \mathbf{J}\Delta X_{cg} + \mathbf{L}_{\omega g}\left[F_{cg}^{\nu+1} - F_{cg}^{\nu}\right]. \tag{23}$$

The solution X_{cg} is computed by iterating the residual, $R^{\nu+1}$ in (23) to zero. To facilitate convergence we use a relaxation parameter λ according to

$$X_{cg}^{\nu+1} = X_{cg}^{\nu} + \lambda\Delta X_{cg}. \tag{24}$$

Note that when the forcing function is linear (independent of X_{cg}), the last term and updated residual in (23) are zero and for $\lambda = 1$, the solution X_{cg} can be evaluated from (24) in one iteration.

IV. Treatment of Time-Dependent Constraints

The time-dependent constraints can be enforced in two ways. The first one enforces the constraints at the GLL grid points since the the spectral element solution, X_{cg} at these points is readily available. The constraint in (2) becomes

$$g_i(\boldsymbol{b}, \boldsymbol{z}(t_j), \dot{\boldsymbol{z}}(t_j), \ddot{\boldsymbol{z}}(t_j), t_j) \le 0, \quad i = 1, ..., n, \quad j = 1, ..., n_g, \tag{25}$$

where n_g is the total number of grid points. In this approach, the grid points need to be closely spaced to reduce potential of constraint violation between adjacent grid points. However, this causes the number of points or constraints to be excessively large and leads to an expensive design process. The second one enforces the time constraints at its most critical time points (extrema) [12,13]. The constraint in (2) becomes

$$g_i(\boldsymbol{b}, \boldsymbol{z}(t_j), \dot{\boldsymbol{z}}(t_j), \ddot{\boldsymbol{z}}(t_j), t_j) \leq 0, \quad i = 1, ..., n, \quad j = 1, ..., n_c, \tag{26}$$

where n_c is the number of local extrema or critical points. Once an accurate low degree of freedom spectral element solution is constructed, the local extrema of the Lagrange polynomial within each element is found using a one dimensional optimization method. Note that the location of the critical time points may drift as $\boldsymbol{b}$ is iterated. Therefore the extrema locations are recomputed during the design process.

V. Sensitivity Analysis

The temporal spectral element method reduces the differential equation of motion to an algebraic form resembling static equations $Ku = f$. Assuming we are applying the constraints at the GLL points according to (25), we can write the constraint as

$$h = g(X_{cg}, b) \leq 0, \tag{27}$$

where for simplicity of discussion we assume h depends on one design variable b. The sensitivity of h to a change in b is

$$\frac{\mathrm{d}h}{\mathrm{d}b} = \frac{\partial g}{\partial b} + \boldsymbol{y}^T \frac{\mathrm{d}X_{cg}}{\mathrm{d}b}, \tag{28}$$

where $\boldsymbol{y}$ is a vector with components

$$y_i = \frac{\partial g}{\partial X_{cg_i}}. \tag{29}$$

The first term in (28) is usually zero or simple to evaluate. The second part can be computed directly by differentiating (20) with respect to b and collecting multipliers to the response sensitivity $\frac{\mathrm{d}X_{cg}}{\mathrm{d}b}$

$$(\mathbf{J} + \mathbf{L}_{\omega g}\mathbf{Q})\frac{\mathrm{d}X_{cg}}{\mathrm{d}b} = -\mathbf{L}_{\omega g}\frac{\partial F_{cg}}{\partial b} - \frac{\mathrm{d}\mathbf{J}}{\mathrm{d}b}X_{cg}, \tag{30}$$

where the matrix $\mathbf{Q}$ is

$$Q_{ij} = \frac{\partial F_{cg_i}}{\partial X_{cg_j}}. \tag{31}$$

Note that for a linear forcing function $\mathbf{Q} = 0$. The sensitivity is computed by solving (30) for $\frac{\mathrm{d}X_{cg}}{\mathrm{d}b}$ and substituting into (28). Alternatively, the sensitivity can be computed using the adjoint method [1, page 265] without the need to compute the sensitivity of the response. By premultiplying (30) with a Lagrange multiplier $\boldsymbol{\lambda}$, adding it to (28) and collecting multipliers to the response sensitivity $\frac{\mathrm{d}X_{cg}}{\mathrm{d}b}$ we have

$$\frac{\mathrm{d}h}{\mathrm{d}b} = \frac{\partial g}{\partial b} + \left[\boldsymbol{y}^T + \boldsymbol{\lambda}^T(\mathbf{J} + \mathbf{L}_{\omega g}\mathbf{Q})\right]\frac{\mathrm{d}X_{cg}}{\mathrm{d}b} + \boldsymbol{\lambda}^T\left(\mathbf{L}_{\omega g}\frac{\partial F_{cg}}{\partial b} + \frac{\mathrm{d}\mathbf{J}}{\mathrm{d}b}X_{cg}\right), \tag{32}$$

where to eliminate the need to compute $\frac{\mathrm{d}X_{cg}}{\mathrm{d}b}$, the adjoint vector $\boldsymbol{\lambda}$ becomes the solution to

$$\boldsymbol{y}^T = -\boldsymbol{\lambda}^T(\mathbf{J} + \mathbf{L}_{\omega g}\mathbf{Q}). \tag{33}$$

The sensitivity is then computed by dropping out the term containing $\frac{\mathrm{d}X_{cg}}{\mathrm{d}b}$ in (32)

$$\frac{\mathrm{d}h}{\mathrm{d}b} = \frac{\partial g}{\partial b} + \boldsymbol{\lambda}^T\left(\mathbf{L}_{\omega g}\frac{\partial F_{cg}}{\partial b} + \frac{\mathrm{d}\mathbf{J}}{\mathrm{d}b}X_{cg}\right). \tag{34}$$

The choice of the constraint(s) sensitivity computation method depends on the number of constraints and design variables [1, page 267]. When the number of constraints is larger than the number of design variables it is more efficient to use the direct method by solving (30) for $\frac{\mathrm{d}X_{cg}}{\mathrm{d}b}$ once for each design variable and substituting into (28). Otherwise, when the number of design variables is larger, the adjoint method is more efficient to use by computing the adjoint vector in (33) once for each constraint and substituting into (34).

VI. Results and Discussion

Two example problems are employed to demonstrate dynamic response optimization for transient and periodic analysis.

VI.A. Impact Absorber

We describe an example of the dynamic response for a single-degree-of-freedom linear impact absorber studied by Etman et al. [17]. The optimization problem is solved using the analytical solution and a spectral element approximation of the solution in time. The analytical solution is used to evaluate the accuracy of the temporal spectral element approach. In this example we compare two approaches for applying the time-dependent constraints with regard to accuracy and efficiency. In the first one, the constraints are enforced at the Gauss-Lobatto-Legendre, GLL, grid points. Here large number of points are needed to reduce greatly opportunity for constraint violation between any two adjacent points. In the second approach, we enforce the constraints only at the global minimum of the time response. This comparison is provided to show the computational cost incurred and design accuracy of both approaches.

The impact absorber is modeled as a single degree of freedom system with a mass M, linear stiffness K and linear damping coefficient C see Figure 2. The differential equation describing the motion of the absorber mass for zero initial displacement and velocity of 1 m/s is

$$M\ddot{z} + C\dot{z} + Kz = 0, \qquad z(0) = 0 \text{ m}, \qquad \dot{z}(0) = 1 \text{ m/s}. \tag{35}$$

The analytical solution of (35) for different combinations of stiffness and damping is

$$z(K,C,M,t) = \begin{cases} \frac{e^{-t\frac{C}{2M}}}{\sqrt{\frac{K}{M}-(\frac{C}{2M})^2}} sin\left(t\sqrt{\frac{K}{M}-(\frac{C}{2M})^2}\right), & \text{if } 0 \le \frac{C/(2M)}{\sqrt{K/M}} < 1; \\ te^{-t\sqrt{\frac{K}{M}}}, & \text{if } \frac{C/(2M)}{\sqrt{K/M}} = 1; \\ \frac{e^{-t\frac{C}{2M}}}{2\sqrt{(\frac{C}{2M})^2-\frac{K}{M}}}\left[e^{t\sqrt{(\frac{C}{2M})^2-\frac{K}{M}}} - e^{-t\sqrt{(\frac{C}{2M})^2-\frac{K}{M}}}\right], & \text{if } \frac{C/(2M)}{\sqrt{K/M}} > 1; \end{cases} \tag{36}$$

For a fixed mass of the impact absorber ($M = 1$ kg), the optimization problem of the absorber is to find the stiffness b_1 and damping coefficient b_2 combination that minimizes the maximum acceleration of the mass in the time interval $t \in [0, T]$

$$f(\boldsymbol{b}) = max|\ddot{z}(\boldsymbol{b}, t)|, \tag{37}$$

subject to the time displacement constraint

$$g(\boldsymbol{b}) = |z(\boldsymbol{b}, t)| - 1 \le 0 \qquad \forall t \in [0, T], \tag{38}$$

and side constraints of the design variables

$$0 \le \boldsymbol{b} \le 1. \tag{39}$$

We note here that the time constraint has to be satisfied for time interval. A time period $T = 12$ s is used which includes all important response characteristics. A graphical representation of the optimization problem is depicted in Figure 3. The maximum acceleration contours are plotted with the displacement constraint. The hatched part of the displacement constraint denotes the region where the constraint is violated. The design which minimizes the maximum acceleration is where the constraint intersects the minimum value of the objective function. For computational purposes the optimization problem is reformulated by minimizing an artificial design variable b_3 [18]

$$f(\boldsymbol{b}) = b_3, \tag{40}$$

subject to acceleration and displacement constraints

$$\begin{aligned} g_1(\boldsymbol{b}) &= \ddot{z}(b_1, b_2, t) - b_3 \le 0, \\ g_2(\boldsymbol{b}) &= -\ddot{z}(b_1, b_2, t) - b_3 \le 0, \\ g_3(\boldsymbol{b}) &= z(b_1, b_2, t) - 1 \le 0, \\ g_4(\boldsymbol{b}) &= -z(b_1, b_2, t) - 1 \le 0, \end{aligned} \tag{41}$$

where

$$0 \le b_1 \le 1, \quad 0 \le b_2 \le 1, \quad b_3 \ge 0, \quad \forall t \in [0, 12].$$

The optimum design is first computed using the analytical solution in (36). The time constraints in (41) are applied at the most critical point in the displacement and acceleration responses. The critical point is found by implementing a one dimensional optimization search. The optimization search method is the sequential quadratic programming (SQP) algorithm which is implemented using the *fmincon* function in Matlab. The accuracy in the objective, constraints and design variables is set to 1×10^{-15} in the main optimization and for locating the critical point. Note that the location of the critical time point is not constant and will continue to change as the design variables change. The optimum design, $\boldsymbol{b}_{\text{analytic}} = \{0.3606 \text{ N/m}, 0.4851 \text{ N.s/m}, 0.5206 \text{ m/s}^2\}$, is noted with green circle in Figure 3. This design is used to compare the accuracy of the design obtained when the temporal spectral element method is used to compute the acceleration and displacement responses.

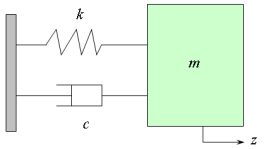

Figure 2. Impact absorber.

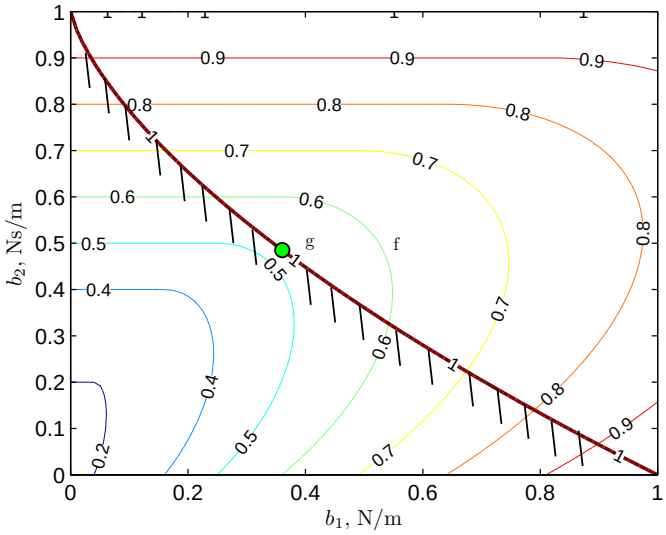

Figure 3. Maximum acceleration contours and displacement constraint for impact absorber. The optimum design is noted by green circle.

The spectral element solution of (35) is computed by transforming the second order differential equation to first order. To facilitate this we introduce variables $z_1 = \dot{z}$ and $z_2 = z$ into (35) to get

$$\begin{Bmatrix} \dot{z_1} \\ \dot{z_2} \end{Bmatrix} + \begin{bmatrix} M & 0 \\ 0 & 1 \end{bmatrix}^{-1} \begin{bmatrix} C & K \\ -1 & 0 \end{bmatrix} \begin{Bmatrix} z_1 \\ z_2 \end{Bmatrix} = \begin{Bmatrix} 0 \\ 0 \end{Bmatrix}, \tag{42}$$

and after matrix multiplication, the first order form becomes

$$\begin{Bmatrix} \dot{z_1} \\ \dot{z_2} \end{Bmatrix} + \begin{bmatrix} C/M & K/M \\ -1 & 0 \end{bmatrix} \begin{Bmatrix} z_1 \\ z_2 \end{Bmatrix} = \begin{Bmatrix} 0 \\ 0 \end{Bmatrix}. \tag{43}$$

The acceleration response, $\dot{z}_1$, needed for the objective function evaluation can be computed from (43) after computing the velocity and displacement responses.

The constraints in (41) can then be written as

$$\begin{aligned} g_1(\boldsymbol{b}) &= \dot{z_1}(b_1, b_2, t) - b_3 \leq 0, \\ g_2(\boldsymbol{b}) &= -\dot{z_1}(b_1, b_2, t) - b_3 \leq 0, \\ g_3(\boldsymbol{b}) &= z_2(b_1, b_2, t) - 1 \leq 0, \\ g_4(\boldsymbol{b}) &= -z_2(b_1, b_2, t) - 1 \leq 0, \end{aligned} \tag{44}$$

where,

$$0 \leq b_1 \leq 1, \quad 0 \leq b_2 \leq 1, \quad b_3 \geq 0, \quad \forall t \in [0, 12].$$

From (42) and using the chain rule the sensitivities of g_1 and g_3 are

$$\begin{aligned} \frac{\partial g_1}{\partial b_1} &= -\frac{1}{M}(z_2 + b_1 \frac{\partial z_2}{\partial b_1} + b_2 \frac{\partial z_1}{\partial b_1}), & \frac{\partial g_3}{\partial b_1} &= \frac{\partial z_2}{\partial b_1}, \\ \frac{\partial g_1}{\partial b_2} &= -\frac{1}{M}(z_1 + b_2 \frac{\partial z_1}{\partial b_2} + b_1 \frac{\partial z_2}{\partial b_2}), & \frac{\partial g_3}{\partial b_2} &= \frac{\partial z_2}{\partial b_2}, \\ \frac{\partial g_1}{\partial b_3} &= \{-1\}, & \frac{\partial g_3}{\partial b_3} &= \{0\}. \end{aligned} \tag{45}$$

The sensitivity is computed by the adjoint method using (34) by solving for the adjoint vector once for the two constraints (g_1 and g_3).

In the initial spectral element implementation, the time constraints are monitored at all GLL points. In this procedure we may need to use large number of time grid points in order to capture the extremum of the response. In Table 1, the infinity error norm of the optimum design $||\boldsymbol{b} - \boldsymbol{b}_{\text{analytic}}||_\infty$ is reported along with the corresponding computational time for different number of elements and Lagrange polynomial order. The accuracy of the design fluctuates and largely depends on whether a particular grid point is at the maximum of the response. For example, Figure 4a shows grid points for one element and degree eleven Lagrange polynomial, where none of the grid points were located at the maximum of the response. During design iterations the grid points may come close to the maximum response, though this situation cannot be predicted in advance of the design process, an example of this is reported in Figure 4b at the optimum design. The best accuracy was obtained at $N_{el} = 105$ and $m = 3$. The computational time of the optimization run for forward finite-difference and adjoint sensitivity computation is additionally noted. The latter method is slightly more efficient than the finite-difference perturbation of the responses. Though, for larger number of design variables, the cost savings of the adjoint approach is still realizable. This is because, the cost of the adjoint sensitivity is dominated by the computational cost of computing the adjoint vector using (33), which is independent of the number of design variables. The reported time corresponds to a computation using Matlab *backslash* operator, which uses an LU factorization based on Gaussian elimination.

Alternatively, we can apply the time constraints only at the critical points of the time response while the response is computed using minimal number of degrees of freedom corresponding to an acceptable accuracy at each grid point. To find the critical times, we use a one dimensional optimization search to locate the local extrema of the corresponding Lagrange polynomial within each element, see the one element solution in Figure 4. Here the *fmincon* function is used with the accuracy in the objective and time design variable being set to 1×10^{-15} for the critical point search. The constraint is then enforced at each local minimum. To locate all the local extrema we run *fmincon* with multiple initial guesses corresponding to the grid points close to these extrema. However, for this problem, there is only one global minimum and we apply the constraint at this point only whilst the location of this point will be updated as the design variables change during optimizer iterations. Table 2, reports the infinity error norm of the computed design and the corresponding computational time for combinations of Lagrange polynomial order and number of elements. The data indicate that the accuracy and efficiency improved substantially with small number of elements and polynomial degree in comparison to the previous approach. Particularly, the design was accurate to 1.9×10^{-9} with $m = 14$ and $N_{el} = 2$. This indicates superiority of applying time-dependent constraints at the critical extrema of the response with regard to computational cost and accuracy.

VI.B. Control Force Design Considering Minimum Work

An interesting application of dynamic response optimization is in the design of micro air vehicles (MAV)[19–21]. One aspect in the design of MAV is the selection of a control force that minimizes utilization of actuation

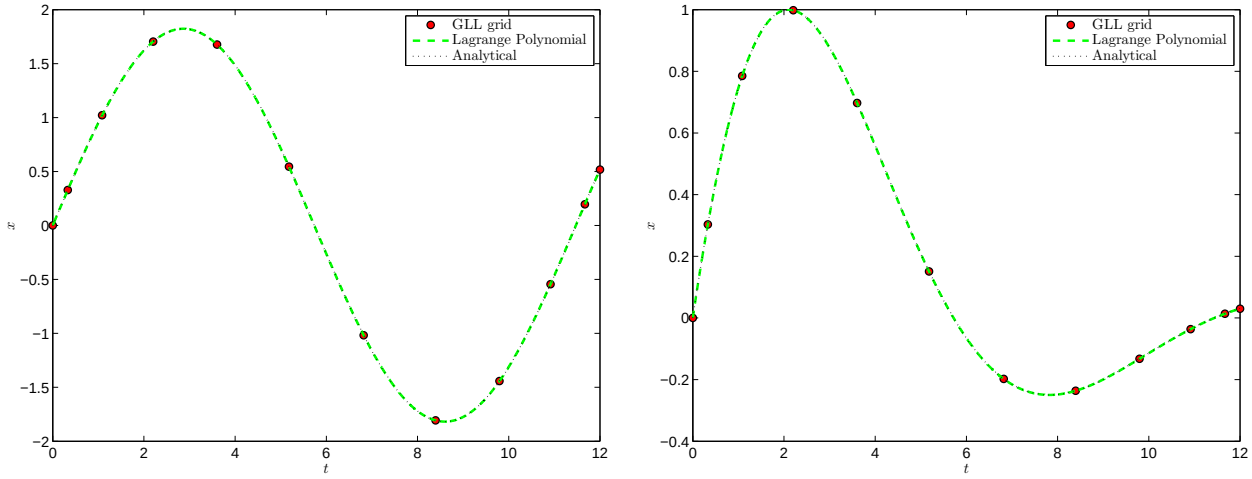

(a) Grid point far from maximum response

(b) Grid point close to maximum response, (optimum design)

Figure 4. Underdamped response of impact absorber. The uneven spacing of GLL grid points for an eleven degree polynomial element are noted.

Table 1. Infinity error norm of the design when the constraints and objective are evaluated at the GLL nodal points. The analytic design corresponds to the design computed using critical time points with analytical objective and constraints. The CPU computation time is noted.

		$\|\|\frac{\boldsymbol{b}-\boldsymbol{b}_{\text{analytic}}}{\boldsymbol{b}_{\text{analytic}}}\|\|_\infty$ %									
		N_{el}									
		5	30	55	80	105	130	155	180	205	230
m	1	177.320	2.146	2.357	2.701	1.449	0.391	0.399	0.951	1.032	0.432
	2	12.177	2.784	0.519	1.545	0.800	0.176	0.188	0.456	0.663	0.101
	3	10.453	0.434	1.015	0.377	0.065	0.462	0.323	0.081	0.195	0.463
Adjoint sensitivity - CPU time, s											
m	1	0.1	0.5	0.3	0.5	0.7	0.7	0.9	1.4	1.3	1.6
	2	0.1	0.3	0.6	1.1	1.3	2.2	2.5	3.2	4.0	5.1
	3	0.1	0.5	0.8	2.0	3.0	4.2	6.1	8.2	8.8	10.7
finite-difference sensitivity - CPU time, s											
m	1	0.1	0.5	0.4	0.7	0.9	1.0	1.2	1.7	1.7	2.1
	2	0.2	0.4	0.7	1.5	1.8	2.7	3.2	3.8	4.9	5.9
	3	0.2	0.6	1.1	2.6	3.4	4.8	7.5	9.4	10.6	12.9

Table 2. Infinity error norm of the design when the global minimum approach is used to enforce the constraints with finite difference sensitivity. The temporal spectral element method is used to compute the responses. The analytic design corresponds to the design computed with analytical objective and constraints. The CPU computation time is noted.

		$\|\|\frac{\boldsymbol{b}-\boldsymbol{b}_{\text{analytic}}}{\boldsymbol{b}_{\text{analytic}}}\|\|_\infty$ %					CPU time, s				
		m					m				
		6	8	10	12	14	6	8	10	12	14
N_{el}	1	1.8×10^{2}	3.0×10^{-1}	2.2×10^{-2}	8.6×10^{-4}	9.3×10^{-6}	2.1	2.3	2.4	2.9	2.7
	2	1.6×10^{-1}	3.2×10^{-3}	2.5×10^{-5}	1.0×10^{-6}	1.9×10^{-7}	2.4	2.6	2.5	2.9	3.0
	3	1.2×10^{-2}	8.6×10^{-5}	1.6×10^{-6}	2.0×10^{-6}	8.3×10^{-7}	2.5	2.5	2.9	3.0	3.2

work[22, 23]. A simplified model of the MAV is a mass-spring-damper system. When the system is linear, the long time response of the underdamped system is independent of the initial conditions. The response to a periodic actuation force is governed by the differential equation

$$M\ddot{z} + C\dot{z} + Kz = f(t+T), \tag{46}$$

where T is the period of the actuation force f. Writing Eq. 46 in scaled time $s \in [0, 1]$

$$\frac{1}{T^2}M\ddot{z} + \frac{1}{T}C\dot{z} + Kz = f(s), \tag{47}$$

where $\dot{z}$ is now the derivative with respect to s. To compute the response z using the SE method, Equation 47 is written in first-order form similar to (42)

$$\frac{1}{T^2}\begin{Bmatrix}\dot{z_1}\\ \dot{z_2}\end{Bmatrix} + \begin{bmatrix}M & 0\\ 0 & 1\end{bmatrix}^{-1}\begin{bmatrix}\frac{C}{T} & K\\ -\frac{1}{T^2} & 0\end{bmatrix}\begin{Bmatrix}z_1\\ z_2\end{Bmatrix} = \begin{bmatrix}M & 0\\ 0 & 1\end{bmatrix}^{-1}\begin{Bmatrix}f(s)\\ 0\end{Bmatrix}. \tag{48}$$

The actuation force $f(s)$ is modeled using a cubic spline discretization. This ensures first derivative continuity of the force and makes and accurate time integration less costly. The alternative option of discretizing the force at all the GLL points results in inaccurate time integration, where perturbations in the actuation force (design variables) during design iterations would result in sharp variations in the actuation force at interelement nodes. Sharp change in the actuation force may not be realizable and may cause inaccuracies in the time integration resulting in an erroneous optimization search. Note that an increase in the number of elements will only deteriorate time integration accuracy by allowing extra points of sharp change. The spline simulation of the actuation force is constructed by enforcing C^1 continuity at a number of nodes on the scaled time interval of [0,1]. Design points are assigned to the magnitude of the actuation force at each node. Since we are implementing a periodic analysis, the magnitude of the force at the left boundary node ($s = 0$) must be equal to the one at the right boundary node ($s = 1$). This can be enforced by assigning the same design variable to both nodes at $s = \{0, 1\}$.

The number of nodes is selected to enable an accurate construction of different variations of the actuation force. This allows for the precise interpolation of the force magnitude to the GLL grid points. For example, when 10 design points are used to construct the function $\arctan(10 \sin 2\pi s)/1.5$ (Figure 5a), there exist large differences between the original function and the spline fitted one. This error will result in an error in the value of function at the GLL grid points (F_{cg}). When the number of design points is increased, the interpolation error is reduced, see Figure 5b, and the spectral element solution accuracy is improved.

Once the GLL grid points are computed from the spline interpolation, it is important that the number of GLL points be adequate in reconstructing the actual actuation force represented by the spline. This is particulary important when design perturbations of design points lead to an actuation force with high frequency content, where we need to ensure the convergence of the SE discretization in all of the control force design space. Consider for example the spline representation of the harmonic $\sin 2\pi s$. The spline is constructed using 51 design points ($n_d = 51$, with one design variable reserved for the control force period) using the values $\sin 2\pi s_i$. A spectral discretization using a Lagrange polynomial of order $m = 5$ and $N_{el} = 5$ (25 grid points) is used to construct the $\sin 2\pi s$ signal. Figure 6a, illustrate good accuracy of the

signal reconstruction using the 25 GLL grid points as seen by the overlapping of the spline and Lagrange interpolations. In the design optimization search the design variables are frequently perturbed. This can be simulated by adding a Gaussian noise of $N(\mu, \sigma)\delta$ with $\delta = 0.2$, $\mu = 0$ and $\sigma = 1$ to each design point. This results in a high frequency actuation force. Now, when the 25 GLL grid points are used to reconstruct the actuation force significant error is introduced, see Figure 6b. The error is due to insufficient number of GLL grid points for the iterated design. The error is reduced by ensuring that the number of GLL grid points are at least equal to the number of control force design points $(n_d - 1)$ see Figrue 6c.

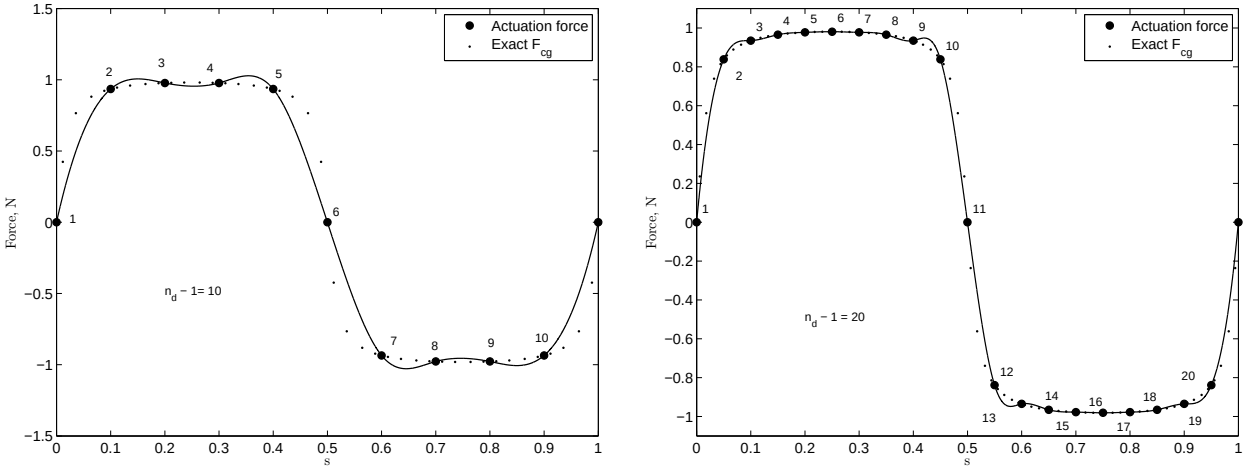

(a) 10 design points

(b) 20 design points

Figure 5. Effect of the number of design points $(n_d - 1)$ on the accurate simulation $\arctan(10 \sin 2\pi s)/1.5$. The interpolation error of the force values at GLL points (F_{cg}) is reduced by increasing n_d.

The optimization problem is to find the period, T and functional form of the control force that minimizes the exerted work for a specified set of target steady-state displacement amplitudes, Z_{T_i}

$$\min_{T, F_d} \quad W \qquad d = 1, ..., n_d - 1, \tag{49a}$$

subject to

$$\max(|z|) \geq Z_{T_i} \qquad i = 1, ..., N, \tag{49b}$$

$$|F_d| \leq 1, \tag{49c}$$

$$\frac{T_n}{4} < T \leq 4T_n, \tag{49d}$$

where W is the amount of external work per cycle exerted by $f(s)$

$$W = \int_0^1 f(s)\dot{z}ds, \tag{50}$$

and F_d is the magnitude of the control force at design node d, n_d is the total number of design variables which include the period T and T_n is the natural period of the system. The minimum work per cycle objective is motivated by the MAV, where an optimal actuation force is favorable to achieve a prescribed maximum displacement amplitude with the least amount of work.

The above optimization problem is solved using a gradient-based optimization method provided by the *fmincon* function in Matlab, where the gradient of the objective function is used to guide the optimization search. Here we compute the gradient using direct perturbation of the objective function and focus on numerical issues associated with finite-difference techniques. We reserve the use of the efficient adjoint method for future investigations. Finite-difference methods are used to estimate the gradient with respect to each design variable, F_d according to

$$\frac{\partial W}{\partial F_d} = \frac{W(F_d + \delta F) - W(F_d - \delta F)}{2\delta F}. \tag{51}$$

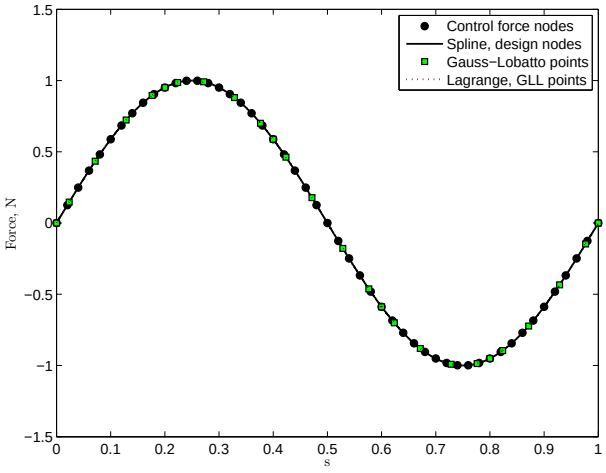

(a) $\sin 2\pi s_i$ with $N_{el} = 5$ and $m = 5$.

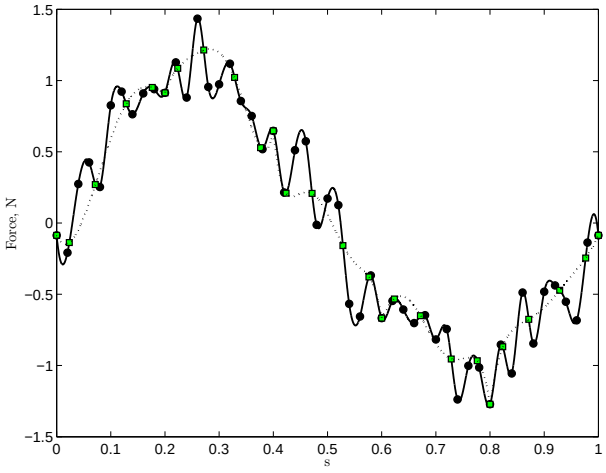

(b) $\sin 2\pi s_i + N(0,1)\delta$ with $N_{el} = 5$ and $m = 5$.

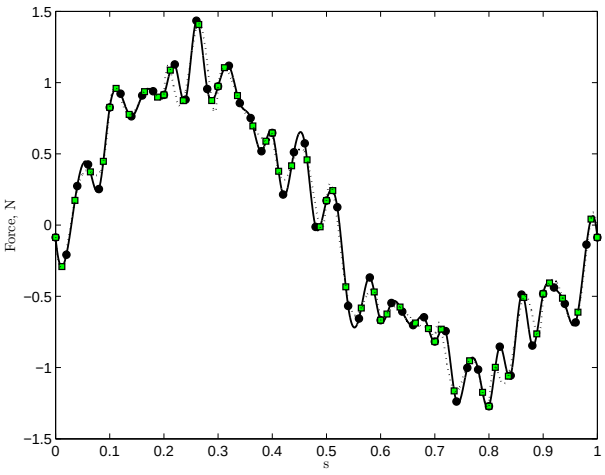

(c) $\sin 2\pi s_i + N(0,1)\delta$ with $N_{el} = 10$ and $m = 5$.

Figure 6. Inaccurate time integration due to under-resolution in the spectral element discretization for a design perturbation.

Because W is not available analytically, its value is estimated using trapezoidal-rule of integration. A numerical error ϵ_w results due to this integration. When the number of control force design variables increases, the round-off error start to dominate the computed value of W and ϵ_w becomes significant [1, page 257]. This causes the gradient to exhibit a numerical noise. A smoothing can be applied to filter out the numerical noise [24], where the smoothed gradient $\bar{G}$ is computed from the calculated gradient G according to

$$\bar{G} - \epsilon \frac{\partial^2 \bar{G}}{\partial s^2} = G. \tag{52}$$

The smoothing parameter ϵ is selected to average out the numerical noise without losing significant information in G. In implementing the finite-difference smoothing in Eq. 52, we note because of the periodic boundary condition, the gradient at $(s = 0)$ is equal to the gradient at $s = 1$.

Before running the optimization algorithm we normalize the objective function, displacement constraints and range of design variables, this allows an efficient optimization search. Here we normalize the objective function and displacement by the difference of their corresponding values at the natural period and $T_n/4$ of the system, and the initial control force. Parameters which remain fixed in all the following calculations are listed in Table 3. Now, we report results of the optimization search for a smoothed and non-smoothed gradient, and different initial guesses of the period and functional form of the forcing function.

Table 3. Fixed parameters of the control force problem.

M (kg)	K (N/m)	C (N.s/m)	T_n (s)	n_d	m	N_{el}
0.010	10	0.012	0.199	31	5	30

We study the effect of using a smoothing operator in the objective function gradient, and different initial guesses of control force functional forms and period on the optimization search. Table 4 reports on the optimization search computational cost and the converged optimum of objective function. The *fmincon* function uses a sequential quadratic programming algorithm. In the table we report the number of cost function evaluations and number of iterations of the algorithm. Four functional forms of the initial control force are considered with and without gradient smoothing. A constant initial period of $T_i = 1.75T_n$ is used for the computations with different forms of the initial control force guess using smoothed and non-smoothed objective gradient. The effect of gradient smoothing seem to slow down the optimization search by requiring extra number of function evaluations (though the global minimum is only achieved through smoothing). This may be due to the decrease in the gradient magnitude when the smoother is used as shown in Figure 7. The design iterations history of the control force are illustrated in Figure 8 for the first two cases in Table 4. The final design of control force is illustrated in Figure 9 for an optimization search starting with an initial guess conforming to the functions $\sin 2\pi s$, $\cos 2\pi s$ and $\arctan(10 \sin 2\pi s)/1.5$ with an $\epsilon = 0.0$. Table 5 reports on the optimization search when there is lack of knowledge in the natural frequency of the system. When the initial forcing period is slightly higher than the natural period of the system $(= 1.1T_n)$, the optimization search is efficient in locating the minimum value of the cost function. The design iterations history is reported in Figure 10 for the first case in Table 5. Different solution path for the control force is shown but for a cost function $W = 1.138$.

To check on the numerical form of the control force for the final design depicted in Figure 8b,d a new optimization search is carried out with the final design of $\epsilon = 0.01$ as an initial guess, but now with non-smoothed gradient. The final solution is reported in Figure 11, where the control force is shown to exhibit oscillations near $s = 0$ with sharper variation at $s = 0.25$ and $s = 0.75$, but no significant improvement in the amount of applied work (third case in Table 4). Furthermore, we consider the effect of increasing the number of control force design points on the control force optimum shape and minimum value of the objective function. Figure 12 indicate that as the number of design points is increased, the control force shape approaches that of square wave. Though, with no improvement in the objective function minimum. The increase in the number of design nodes results in a noisy content in the actuation force as reported in Figure 12b,c. A smoothing is applied to the gradient, where it is found effective in mitigating the noise in the optimum control force especially near $s = 0$ for $n_d = 61$ but less effective for $n_d = 91$.

Finally we run the optimization search for a set of target amplitude displacements. This allows us to compute the tradeoff curve of exerted work and maximum displacement amplitude Z_T. An initial guess of $T_i = 1.2T_n$ and initial control force according to $\arctan(10 \sin 2\pi s)/1.5$ with $\epsilon = 0.01$ are used to compute

Table 4. Effect of smoothing and initial control force form on the optimization search for an initial period $T_i = 1.75T_n$ and target displacement amplitude $Z_T = 1$ m.

function	W N.m	ϵ	T_d/T_n	# function evaluations	iterations
$\cos 2\pi s$	1.124	0	1.06	228	6
$\cos 2\pi s$	1.114	0.01	1.06	267	7
Restart†	111.2	0	1.06	267	7
$\arctan(10 \sin 2\pi s)/1.5$	1.117	0	1.06	260	7
$\arctan(10 \sin 2\pi s)/1.5$	1.108	0.01	1.07	300	8
$\sin 2\pi s$	1.124	0	1.06	234	6
$\sin 2\pi s$	1.111	0.01	1.06	300	8
s	2.589	0	3.80	527	15
s	3.945	0.01	3.80	1213	34

† Restart from the final design of cosine function initial guess with smoothing (second case in table), see comparison in Figure 11.

Table 5. Effect of initial control force period on the optimization search for a target displacement amplitude $Z_T = 1$ m.

T_i/T_n	function	W N.m	ϵ	T_d/T_n	# function evaluations	iterations
1.0	$\sin 2\pi s$	1.138	0	1.05	713	20
1.1	$\sin 2\pi s$	1.134	0	1.05	164	4
0.5	$\sin 2\pi s$	NS†	0	NS†	2513	59
0.5	$\sin 2\pi s$	3.875	0.01	3.78	792	23
1.0	$\cos 2\pi s$	1.137	0	1.05	705	20
1.1	$\cos 2\pi s$	1.134	0	1.05	164	4
0.5	$\cos 2\pi s$	1.235	0	0.98	635	18
0.5	$\arctan(10 \sin 2\pi s)/1.5$	2.701	0	3.00	495	14
1.1	$\arctan(10 \sin 2\pi s)/1.5$	1.113	0	1.06	131	3
0.5	s	2.566	0	4.00	529	15
0.9	s	1.153	0	1.01	1231	36
1.1	s	1.102	0	3.80	612	17
1.5	s	2.793	0	3.96	696	20

† No feasible solution found after the reported number of iterations.

the tradeoff curve (Pareto front), see Figure 13a. The calculation of the tradeoff curve is computationally more expensive than a weighted sum approach, however, it allows the designer to select an optimum design based on his/her preferences, where a small increase in the amount of applied work may yield larger increase in the target displacement. Although, Figure 13a does not show this behavior, we may realize this advantage in a realistic model of the MAV. We note here that the final functional form of the actuation force for all the Pareto set resembles that of a square wave (an example orbit of one Pareto design is reported in Figure 13b for $Z_T = 3.0$ m), however, with slightly different actuation period, T_d. The optimum actuation period, see Table 6, is found larger than the natural period of the system, with the difference decreasing in magnitude (reported results are rounded to three significant figures) with increase in the maximum target amplitude.

Table 6. Pareto front optimal set. The initial work 50.4 N.m and initial displacement 0.69 m correspond to the arctangent function with initial control force period of $1.1T_n$.

Displacement amplitude, m	0.5	1.0	1.5	2.0	2.5	3.0	3.3
Minimum Work, N.m	0.254	1.112	2.575	4.649	7.354	10.780	12.990
T_d/T_n	1.16	1.07	1.04	1.03	1.02	0.99	1.00
Change in amplitude %	72.5	144.9	217.4	289.9	362.3	434.9	478.3
Change in work %	50.4	220.6	510.9	922.4	1459.1	2138.9	2577.4

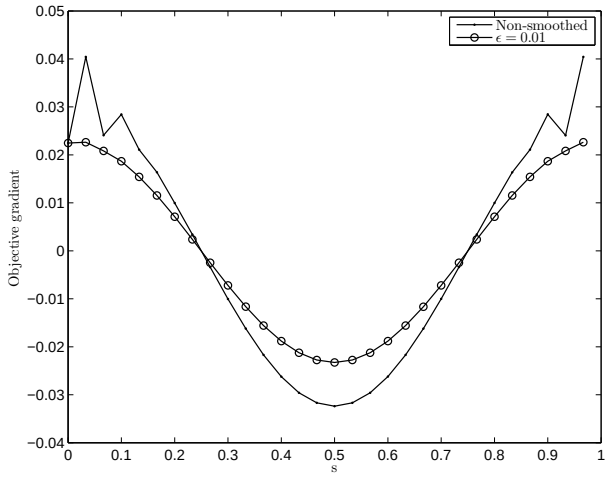

Figure 7. Gradient smoothing for a cosine function initial guess with initial forcing period $T_i = 1.75T_n$

VII. Conclusions

The optimization of systems for dynamic response is valuable in many applications. The performance function and/or constraints are governed by a time-dependent differential equation. In order to apply the time-dependent constraints or find the optimum cost function, the response is required for the whole time interval. In this paper, the response is computed in monolithic time using a spectral element discretization, where the differential equation is transformed to an algebraic form. The search of the optimum design using gradient-based methods is simplified by the availability of the sensitivity of the time-dependent response to a change in the design variables explicitly. The adjoint approach is used to computed the sensitivity and is found more efficient than the finite-difference approach.

Two optimization applications are described, the first one relates to transient analysis, where an impact absorber is designed to minimize the maximum acceleration. In this example we compare the accuracy and efficiency of applying the time-dependent constraints at GLL grid points to applying them at critical points (local extrema). The latter approach proved more efficient and accurate in computing the optimum solution.

The second application covers the periodic steady-state analysis. Here, the control force of a mass-spring-damper system is designed for minimum exerted work and maximum displacement amplitude. The system is a very simplified model of the control of micro air vehicles. The control force is simulated using a

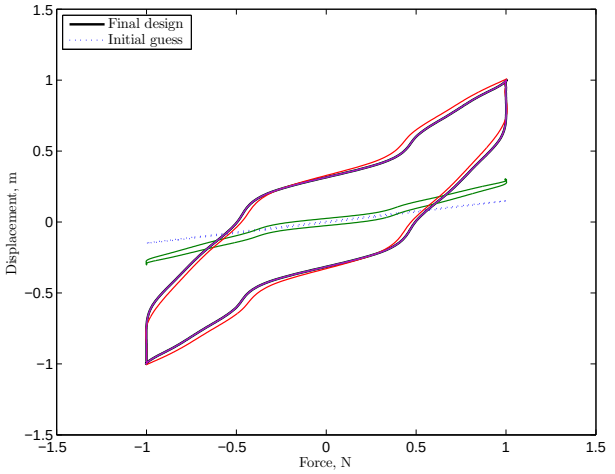

(a) Orbit, non-smoothed gradient, $\epsilon = 0$.

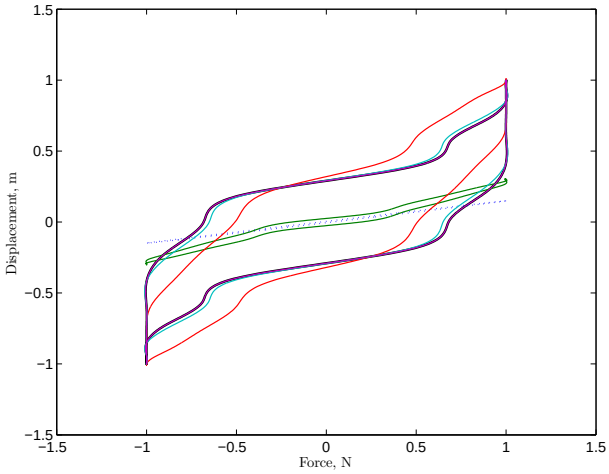

(b) Orbit, smoothed gradient, $\epsilon = 0.01$.

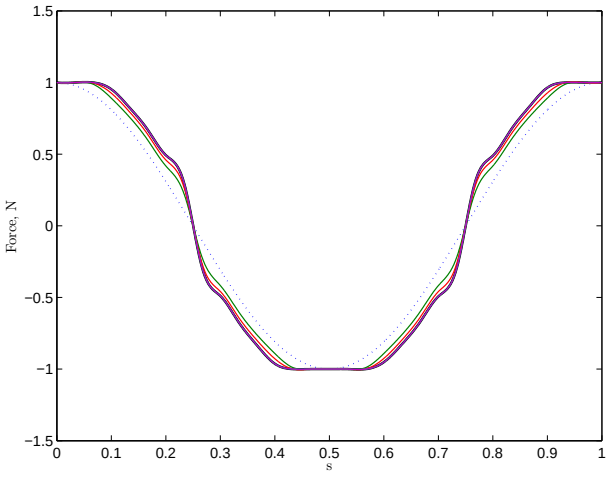

(c) Force, non-smoothed gradient, $\epsilon = 0$.

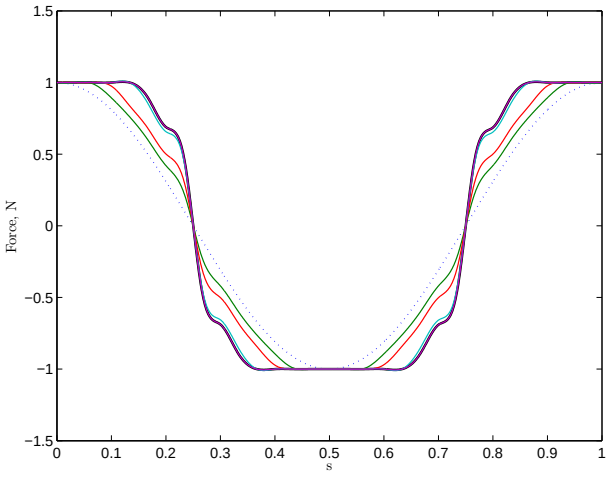

(d) Force, smoothed gradient, $\epsilon = 0.01$.

Figure 8. Design history for a cosine function initial guess with initial forcing period $T_i = 1.75T_n$. Optimum period is $T_d = 1.06T_n$. Only the initial and final design iterations are noted in the legend.

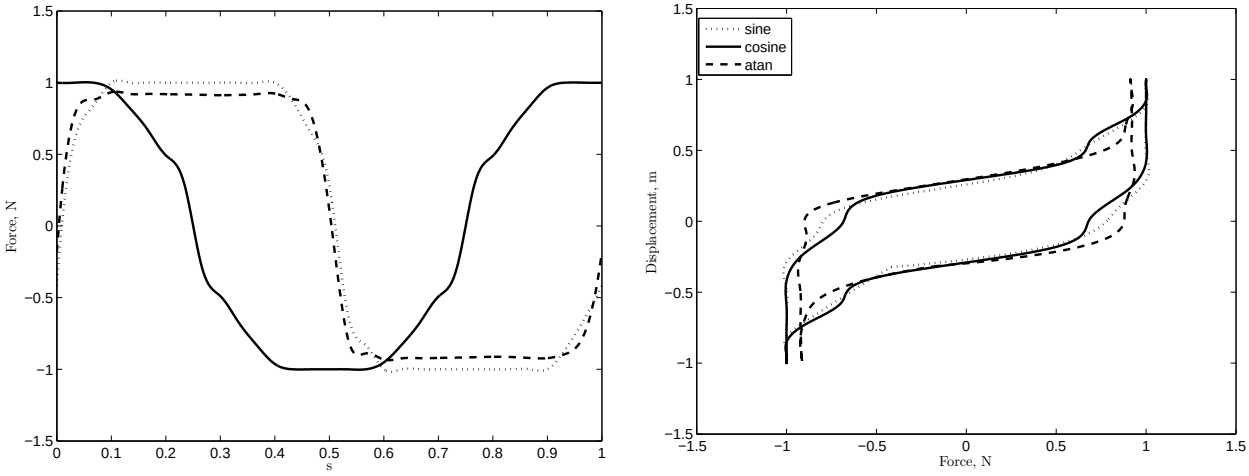

(a) Force. (b) Orbit.

Figure 9. Final design for an initial forcing period $T_i = 1.75T_n$ and different initial forcing function. The applied work for optimum control force path is around 111 N.m. The optimal control force for the arctangent initial guess does not reach the boundary of the control force design space.

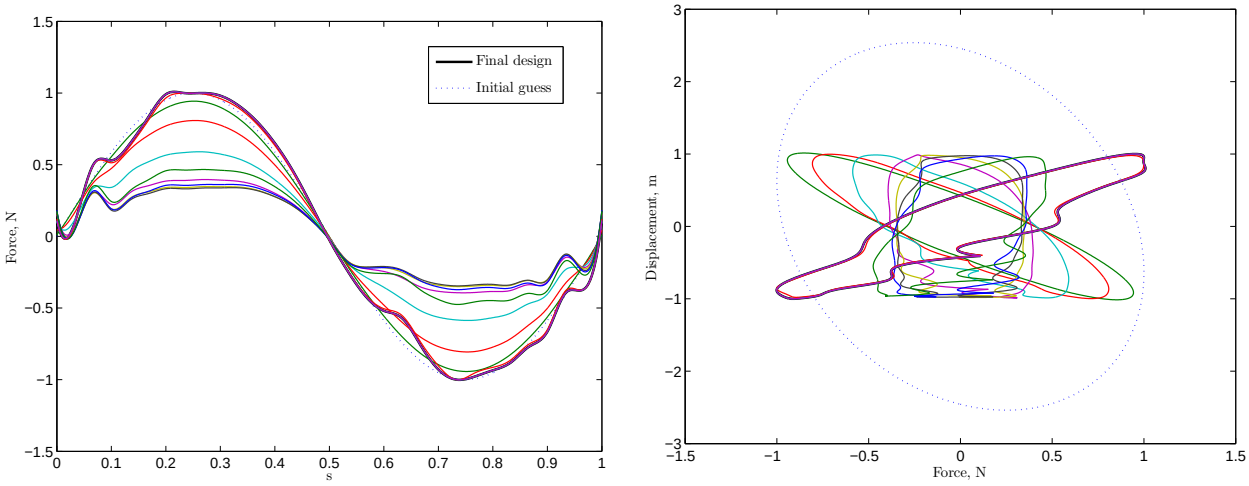

(a) Force. (b) Orbit.

Figure 10. Design history for a sine function initial guess with initial forcing period $T_i = T_n$ and no smoothing. Optimum period is $T_d = 1.05T_n$. Only the initial and final design iterations are noted in the legend.

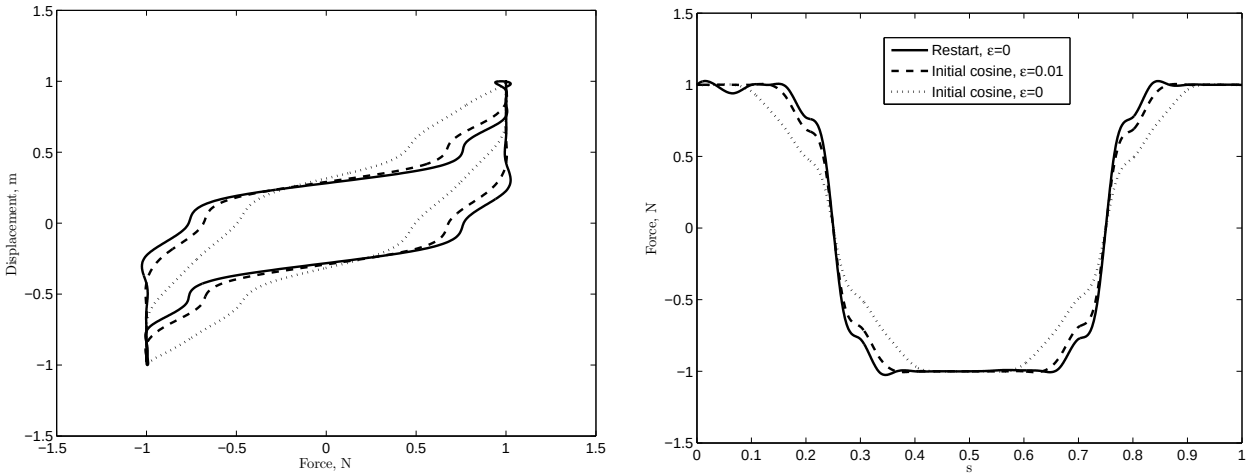

(a) Orbit.

(b) Force.

Figure 11. Final design comparison of the control force for cosine initial control force ($T_i = 1.75T_n$), with $\epsilon = 0$ and $\epsilon = 0.01$, and an initial control force equal to the final design at $\epsilon = 0.01$ but with no smoothing ($\epsilon = 0$)

spline discretization with first derivative continuity, where the design variables are the control force period and the force magnitude at the spline nodes. Time-dependent response is computed for one period of the response using the spectral element method. The study underlined the importance of effective selection in the number of design nodes in the spline and an adequate spectral element discretization. Increasing the number of design nodes in the spline, requires increasing the spectral element discretization to give accurate steady-state response for design perturbations. A high number of design nodes would result in a large round-off error in computing the cost function and contributes to numerical noise in the gradient. Optimization results show that the use of gradient smoothing mitigate noisy oscillations in the control force and favorably improve the final minimum work by 1%, but with an extra number of iterations in comparison with no smoothing. Furthermore, convergence of the optimum solution is found more efficient for a control force period slightly larger than the natural period of the system, with the control force nodes conforming to harmonic and arctangent functions. Finally, the trade-off curve of the minimum work and maximum displacement amplitude is computed. The curve illustrate to the designer the amount of gain in the maximum displacement amplitude corresponding to an available minimum work per cycle. Further research on a better representation of the control force may be required to avoid observed wiggles in the optimum control force shape. Additionally, we would like to consider the effect of variations in the system parameters, especially the natural period, on the optimum control force.

The distinctive feature of the optimization approach used in the paper is the implementation of a high order spectral element computation of the dynamic response in a monolithic time interval which includes the converged dynamics. The approach transforms the differential equation into an algebraic form, which enables a more explicit computation of the sensitivities as highlighted in the review by Kang et. al [3].

Acknowlegment This work is supported by the Air Force Office of Scientific Research under Grant 03VA01COR. We would like to thank our program manager Dr. Fariba Fahroo for her interest and financial support.

References

[1]R.T. Haftka and Z. Gurdal. *Elements of Structural Optimization*. Kluwer Academic Publishers, Dordrecht, The Netherlands, 1992.

[2]C. C. Hsieh and J. S. Arora. Design sensitivity analysis and optimization of dynamic response. *Applied Mathematics and Optimization*, 43(2):195 – 219, 1984.

[3]Byung-Soo Kang, Gyung-Jin Park, and J.S. Arora. A review of optimization of structures subjected to transient loads. *Structural and Multidisciplinary Optimization*, 31(2):81 – 95, 2006.

[4]S. Park, R.K. Kapania, and S.J. Kim. Nonlinear transient response and second-order sensitivity using time finite element

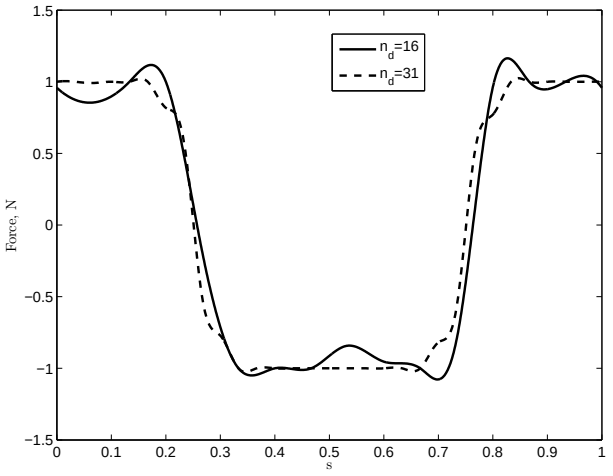

(a) $\epsilon = 0$

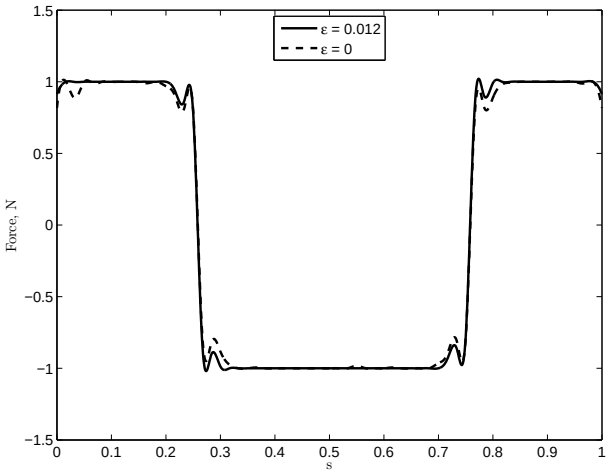

(b) $n_d = 61$

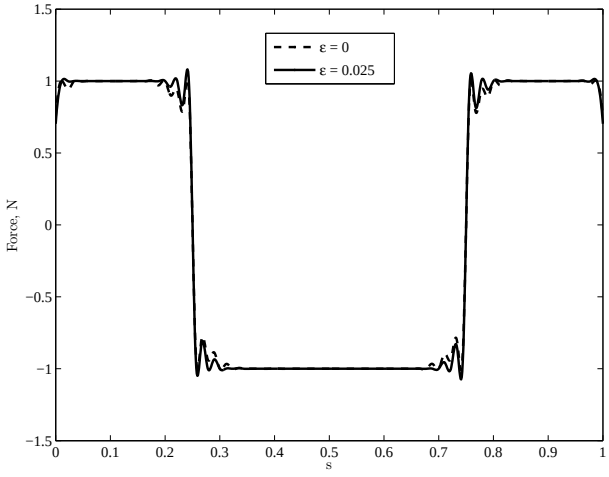

(c) $n_d = 91$

Figure 12. The final design considering a cosine initial control force with $T_i = 1.75T_n$ and different numbers of control force design points. Note because two jumps in the final design, more design nodes are needed. For all cases, the minimum applied work is around 111 N.m with $T_d = 1.07T_n$.

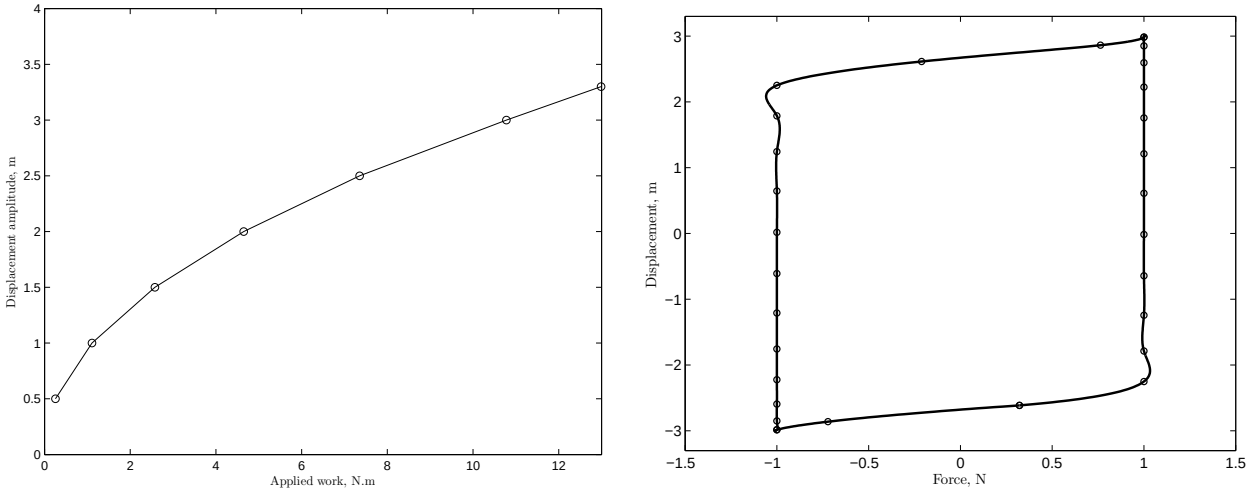

(a) Pareto front

(b) Orbit for $Z_T = 3.0$ m

Figure 13. Pareto front of applied work and target displacement amplitude.

method. *AIAA Journal*, 37(5):613 – 622, 1999.

[5]R.K. Kapania and S. Park. Nonlinear transient response and its sensitivity using finite elements in time. *American Society of Mechanical Engineers, Design Engineering Division (Publication) DE*, 84(3 Pt B/2):931 – 942, 1995.

[6]A.T. Patera. A spectral element method for fluid dynamics; laminar flow in a channel expansion. *Journal of Computational Physics*, 54:468–488, 1984.

[7]M.H. Kurdi and P.S. Beran. Spectral element method in time for rapidly actuated systems. *Journal of Computational Physics*, 227(3):1809–1835, 2007.

[8]K.D. Wilmert and R.L. Fox. Optimum design of a linear multidegree-of-freedom shock isolation system. *Journal of Engineering for Industry*, 94:465 – 471, 1972.

[9]K. A. Afimiwala and R. W. Mayne. Optimum design of an impact absorber. *Journal of Engineering for Industry, Transactions of the ASME*, 96 B(1):124 – 130, 1974.

[10]V.B. Venkayya, N.S. Khot, V.A. Tischler, and Taylor R.F. Design of optimum structures for dynamic loads. In *the 3rd Conference on Matrix Methods of Structural Mechanics*, pages 619–658, Flight Dynamics Laboratory, Wright Patterson Air Force Base, Ohio, October 1971.

[11]R.T. Haftka. Parametric constraints with application to optimization for flutter using a continuous flutter constraint. *AIAA Journal*, 13(4):471–475, 1975.

[12]R.V. Grandhi, R.T. Haftka, and Layne T. Watson. Design oriented identification of critical times in transient response. Number 2, pages 46 – 59, Palm Springs, CA, USA, 1984.

[13]R.V. Grandhi, R.T. Haftka, and L.T. Watson. Efficient identification of critical stresses in structures subject to dynamic loads. *Computers and Structures*, 22(3):373 – 86, 1986.

[14]G.E. Karniadakis and S.J. Sherwin. *Spectral/hp element methods for CFD*. Oxford University Press, 1999.

[15]C. Pozrikidis. *Introduction to finite and spectral element methods using Matlab*. Chapman and Hall/CRC, 2005.

[16]D.S. Burnett. *Finite element analysis; from concepts to applications*. Addison-Wesley, 1988.

[17]L.F.P. Etman, D.H. Van Campen, and A.J.G. Schoofs. Design optimization of multibody systems by sequential approximation. *Multibody System Dynamics*, 2:393–415, 1998.

[18]E.J. Haug and J.S. Arora. *Applied optimal design: mechanical and structural systems*. Wiley-Interscience, New York, 1979.

[19]Wei Shyy, Mats Berg, and Daniel Ljungqvist. Flapping and flexible wings for biological and micro air vehicles. *Progress in Aerospace Sciences*, 35(5):455 – 505, 1999.

[20]R.D. Snyderz M. Blair P.S. Beran, G.H. Parkery. Design analysis strategies for flapping wing micro air vehicles. IFASD AIAA Paper 2007-109, June 18-20.

[21]K. Palaniappan, P.S Beran, and A. Jameson. Optimal control of LCOs in aero-structural systems. AIAA-2006-1621 May 1-4.

[22]M. Kaya and I. H. Tuncer. Path optimization of flapping airfoils based on nurbs. *Parallel Computational Fluid Dynamics*, pages 285–292, 2007.

[23]David L. Raney and Eric C. Slominski. Mechanization and control concepts for biologically inspired micro air vehicles. *Journal of Aircraft*, 41(6):1257 – 1265, 2004.

[24]A. Jameson and J.C. Vassberg. Studies of alternative numerical optimization methods applied to the brachistochrone problem. *Computational Fluid Dynamics*, 9(3):281–296, October 2000.